Applied Energy 87 (2010) 3137–3147

Contents lists available at ScienceDirect

Applied Energy

journal homepage: www.elsevier.com/locate/apenergy

Transport phenomena and performance of a plate methanol steam micro-reformer with serpentine flow field design

Ching-Yi Hsueh [a], Hsin-Sen Chu [a,b], Wei-Mon Yan [c,*], Chiun-Hsun Chen [a]

[a] Department of Mechanical Engineering, National Chiao Tung University, Hsin-Chu 300, Taiwan, ROC
[b] Industrial Technology Research Institute, Chu-Tung, Hsin-Chu 310, Taiwan, ROC
[c] Department of Greenergy, National University of Tainan, Tainan 700, Taiwan, ROC

ARTICLE INFO

Article history:
Received 9 December 2009
Received in revised form 5 February 2010
Accepted 14 February 2010
Available online 8 May 2010

Keywords:
Micro-reformer
Serpentine flow field
Three-dimensional model
Transport phenomena

ABSTRACT

A numerical investigation of the transport phenomena and performance of a plate methanol steam micro-reformer with serpentine flow field as a function of wall temperature, fuel ratio and Reynolds number are presented. The fuel Reynolds number and H_2O/CH_3OH molar ratio (S/C) that influence the transport phenomena and methanol conversion are explored in detail. In addition, the effects of various wall temperatures on the plates that heat the channel are also investigated. The predictions show that conduction through the wall plays a significant effect on the temperature distribution and must be considered in the modeling. The predictions also indicate that a higher wall temperature enhances the chemical reaction rate which, in turn, significantly increases the methanol conversion. The methanol conversion is also improved by decreasing the Reynolds number or increasing the S/C molar ratio. When the serpentine flow field of the channel is heated either through top plate ($Y = 1$) or the bottom plate ($Y = 0$), we observe a higher degree of methanol conversion for the case with top plate heating. This is due to the stronger chemical reaction for the case with top plate heating.

1. Introduction

Fuel cells are widely regarded as the most promising energy systems for transport, stationary and portable power sources due to their properties of high efficiency and high environment compatibility. Many analyses, models and numerical simulations have been developed to study proton exchange membrane fuel cell (PEMFCs) which generate electrical energy from hydrogen [1–4]. In the portable electronics market, fuel cells promise to provide higher power density and longer durability than batteries [5]. Safety issues, storage problems, and size or portability considerations make pure hydrogen feeding relatively difficult for electronic equipment applications. The combination of a methanol reformer with a proton exchange membrane fuel cell (PEMFC) overcomes the high risk involved in carrying a large quantity of hydrogen, and is thus a promising choice for miniaturized portable electronic systems.

The vast literature devoted to the plate methanol steam micro-reformer has been reviewed on several occasions [6–15]. As the steam reforming reaction is an endothermic reaction, several researchers have used an electrical heater to supply heat flux to the plate methanol steam micro-reformers using micro-channels patterned on the plates. This has successfully produced hydrogen to supply the fuel cell [6–10]. A stack of alternate combustion and reforming chambers are separated by plates. Both sides of each plate are coated with a combustion catalyst and a reforming catalyst. The heat from the combustion reaction is used to drive the reforming reaction. As a result, several studies have successfully used catalytic burners to supply thermal energy to the entire micro-reformer which can generate high yields of hydrogen [11–15].

Computational simulation and modeling are used extensively in research and industrial applications to obtain a better understanding of the fundamental processes and to optimize designs before building prototypes for engineering applications. Therefore, more theoretical modeling for study of the methanol reformer is in progress. Suh et al. [16,17] employed a cylindrical mathematical model of a packed bed reformer to investigate heat and mass transport phenomena in a methanol reformer. The results showed good agreement between theoretical and experimental results, and also found that the internally heated reformer could improve the methanol conversion. The effects of the methanol steam reforming rate in both a packed bed reformer and a wall coated reformer were examined by Karim et al. [18,19]. The results showed that a wall coated reformer had better heat and mass transfer limitations and higher catalyst activity than a packed bed reformer. Pan and collaborators [20,21] developed the numerical models for a plate-fin methanol steam reformer and a bench-scale methanol

* Corresponding author. Tel.: +886 6 260 2251; fax: +886 6 260 2205.
E-mail address: wmyan@mail.nutn.edu.tw (W.-M. Yan).

0306-2619/$ - see front matter © 2010 Published by Elsevier Ltd.
doi:10.1016/j.apenergy.2010.02.027

Nomenclature

C_i	concentration of species i (mol m^{-3})
c_p	specific heat at constant pressure
D	hydraulic diameter (m)
D_{eff}	effective mass diffusivity (m^2 s^{-1})
D_k	mass diffusion coefficient (m^2 s^{-1})
D_p	catalyst particle diameter (m)
E_a	activation energy (J mol^{-1})
H	channel height (m)
I, J, K	grid points in the x, y and z directions, respectively
k_{eff}	effective thermal conductivity (W m^{-1} K^{-1})
k_f	fluid phase thermal conductivity (W m^{-1} K^{-1})
k_p	permeability (m^2)
k_s	solid medium thermal conductivity (W m^{-1} K^{-1})
k_1	pre-exponential factor for steam reforming
k_2	pre-exponential factor for the reverse water gas shift
k_{-2}	pre-exponential factor for the water gas shift
ΔH_{SR}	enthalpy of reaction for steam reforming (J mol^{-1})
ΔH_{rWGS}	enthalpy of reaction for the reverse water gas shift (J mol^{-1})
L_s	the total length from the serpentine flow channel inlet to outlet
M_i	mole fraction of species i
$M_{w,i}$	molecular weight of species i (g mol^{-1})
m_i	mass fraction of species i
p	pressure (Pa)
Q_{H2}	hydrogen production rate at outlet (cm^3 min^{-1})
R	universal gas constant
Re	Reynolds number, Re = $\rho u D/\mu$
R_{SR}	Arrhenius reaction rate coefficient for steam reforming (mol m^{-3} s^{-1})
R_{rWGS}	Arrhenius reaction rate coefficient for the reverse water gas shift (mol m^{-3} s^{-1})
S/C	molar ratio of H_2O/CH_3OH
T	temperature (°C)
T_0	inlet temperature (°C)
T_w	wall temperature (°C)
u, v, w	velocity components in the x, y and z directions, respectively (m s^{-1})
W	channel width (m)
X	dimensionless distance from the flow channel inlet to outlet, $X = x_s/L_s$
x, y, z	coordinates (m)
x_s	the length from the serpentine flow channel inlet to outlet (m)
Y	dimensionless coordinate, $Y = y/H$

Greek symbols

β	inertial loss coefficient
δ_1	catalyst layer height (m)
δ_2	flow channel height (m)
θ	dimensionless temperature, $\theta = (T - T_0)/(T_w - T_0)$
ε	porosity
η	methanol conversion
λ_i'	the stoichiometric coefficient for reactant i in reaction
λ_i''	the stoichiometric coefficient for product i in reaction
τ	tortuosity of the porous medium
μ	dynamic viscosity (g m^{-1} s^{-1})
μ_{mix}	viscosity of the gas mixture (g m^{-1} s^{-1})
ϕ_{ij}	an auxiliary term in calculating viscosity of gas mixture
ρ	density (kg m^{-3})

Subscripts

0	inlet

autothermal reformer. Their numerical model accurately predicted the methanol conversion and the gas distribution. A plate micro-reformer model and a radial flow packed bed reformer model were developed by Pattekar and Kothare, respectively [22,23]. The results demonstrated that a radial flow reformer had better hydrogen production rates and lower pressure drops than the micro-channels of a plate reformer. A cylindrical reformer model to simulate the conversion and temperature distribution in the methanol reformer was developed by Cao et al. [24]. Their results showed that the appropriate insulation thickness could reduce the heat losses and achieve a small volume and a high power density. Stamps and Gatzke [25] developed a reformer with a model PEMFC to study various design and operating parameters on system performance. The simplest model to describe the methanol reformer conversion and the heat and mass transport phenomena was presented by Yoon et al. [26]. The results showed that appropriate reactor geometry can improve the reactant gas transport and the efficiency of thermal management. More theoretical modeling of steam reforming coupled with catalytic combustion for the plate reactors is currently in progress. A plate reactor model that combines a steam reformer and catalytic combustor was recently examined by several researchers [27–29]. The systems are fed by hydrocarbons which convert the hydrogen and generate heat. An appropriate numerical model of the micro-reformer with combustor has been developed to explore the heat and mass transport phenomena and conversion efficiency.

In recent years, different types of flow field designs for plate methanol micro-reformers have been used to achieve more efficient methanol conversion. Kundu et al. [30] used different flow configurations, including serpentine and parallel flow fields, to improve plate methanol reformer performance. Several researchers have studied plate steam reformers with a parallel flow field which is attractive due to its simplicity [31–33]. Chen et al. [31] used a plate micro-reformer model to analyze the transport phenomena in a methanol steam reformer. A numerical single channel model to analyze various height and width ratios on the micro-reformer performance and reactant gas transport characteristics was presented by Hsueh et al. [32]. Kim and Kwon [33] proposed a one-dimensional methanol steam reformer model to study the inner transport phenomena. Park et al. [34] presented numerical simulations to study the reforming rate and heat and mass transfer phenomena in a methanol micro-reformer.

The literature cited above has shown that micro-reformer performance can be enhanced by suitable thermo-fluid parameters. However, there has been a limited amount of work investigating the effects of the different flow field designs on thermo-fluid parameters, especially for the serpentine flow field. Therefore, the objective of this paper is to establish a three-dimensional serpentine flow field model of the plate methanol steam micro-reformer to investigate its transport phenomena and methanol conversion efficiency.

2. Analysis

In this study, a three-dimensional computational model of heat and mass transfer in a micro-reformer with a serpentine flow field is proposed. The serpentine flow field has eight turns. A schematic illustration of the coordinate system is shown in Fig. 1. The channel of the serpentine flow field consists of a flow channel and a catalyst

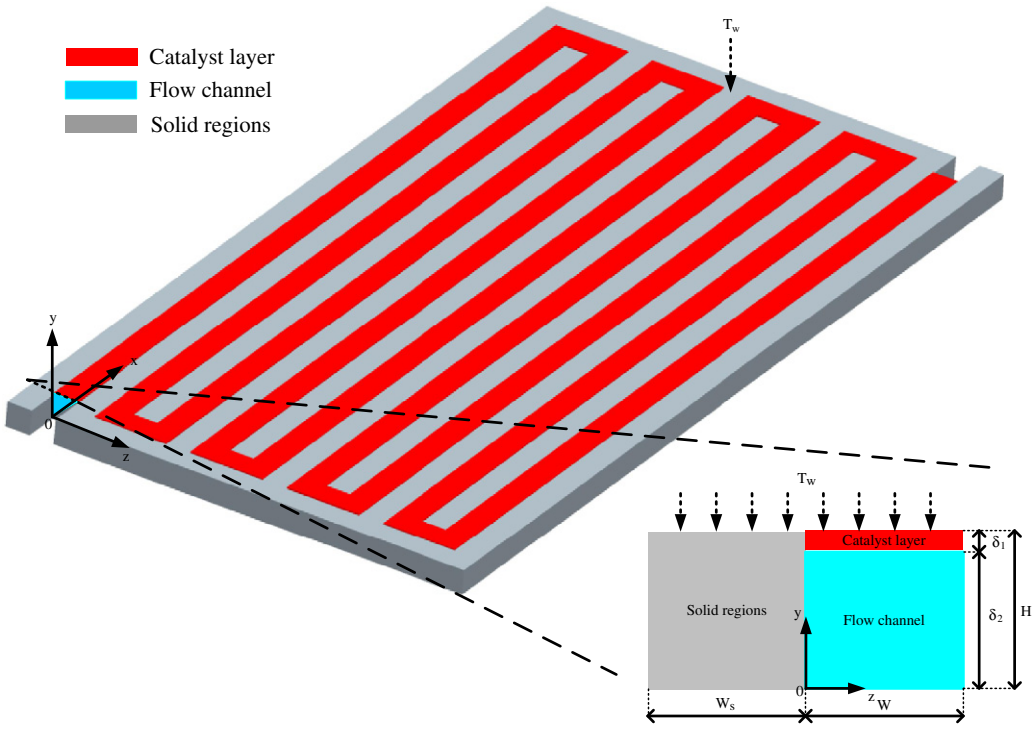

Fig. 1. Schematic diagram of the present study.

layer. In order to simplify the analysis, assumptions are made as follows:

(1) the flow is steady state;
(2) the inlet fuel is an ideal gas;
(3) the flow is laminar and incompressible;
(4) the catalyst layer is isotropic;
(5) the chemical reaction occurs only in the catalyst layer;
(6) thermal radiation and conduction in the gas phase are negligible compared to convection.

According to the descriptions and assumptions above, the basic transport equations for the three-dimensional plate methanol steam micro-reformer are as follows:

Continuity equation:

$$\rho\left(\frac{\partial u}{\partial x}+\frac{\partial v}{\partial y}+\frac{\partial w}{\partial z}\right)=0 \tag{1}$$

X-momentum equation:

$$\varepsilon\rho\left(u\frac{\partial u}{\partial x}+v\frac{\partial u}{\partial y}+w\frac{\partial u}{\partial z}\right)=-\varepsilon\frac{\partial p}{\partial x}+\varepsilon\mu\left(\frac{\partial^2 u}{\partial x^2}+\frac{\partial^2 u}{\partial y^2}+\frac{\partial^2 u}{\partial z^2}\right)+S_u \tag{2}$$

Y-momentum equation:

$$\varepsilon\rho\left(u\frac{\partial v}{\partial x}+v\frac{\partial v}{\partial y}+w\frac{\partial v}{\partial z}\right)=-\varepsilon\frac{\partial p}{\partial y}+\varepsilon\mu\left(\frac{\partial^2 v}{\partial x^2}+\frac{\partial^2 v}{\partial y^2}+\frac{\partial^2 v}{\partial z^2}\right)+S_v \tag{3}$$

Z-momentum equation:

$$\varepsilon\rho\left(u\frac{\partial w}{\partial x}+v\frac{\partial w}{\partial y}+w\frac{\partial w}{\partial z}\right)=-\varepsilon\frac{\partial p}{\partial z}+\varepsilon\mu\left(\frac{\partial^2 w}{\partial x^2}+\frac{\partial^2 w}{\partial y^2}+\frac{\partial^2 w}{\partial z^2}\right)+S_w \tag{4}$$

In the momentum equations, ε is the porosity of the medium. S_u, S_v and S_w are corrected terms for the reactant gas flow in the porous material of the catalyst layer of the micro-reformer. Therefore, S_u, S_v and S_w are different in each computation domain due to the difference in pressure when fluids pass through a porous medium. So, S_u, S_v and S_w in the catalyst layer are:

$$S_u=-\frac{\mu u}{k_p}-\frac{\beta u\rho}{2}\sqrt{u^2+v^2+w^2} \tag{5}$$

$$S_v=-\frac{\mu v}{k_p}-\frac{\beta v\rho}{2}\sqrt{u^2+v^2+w^2} \tag{6}$$

$$S_w=-\frac{\mu w}{k_p}-\frac{\beta w\rho}{2}\sqrt{u^2+v^2+w^2} \tag{7}$$

where k_p is the permeability and β is the inertial loss coefficient in each component direction. In the analysis, the Ergun equations [35] are used to model k_p and β as below:

$$k_p=\frac{D_p^2\varepsilon^3}{150(1-\varepsilon)^2} \tag{8}$$

$$\beta=\frac{3.5(1-\varepsilon)}{D_p\varepsilon^3} \tag{9}$$

where D_p is the diameter of the catalyst particles.

The dynamic viscosity in the gas mixture is calculated from an expression based on kinetic theory as [36]

$$\mu_{mix}=\sum_{i=1}^{5}\frac{M_i\mu_i}{\sum_{j=1}^{5}M_j\phi_{ij}} \tag{10}$$

where

$$\phi_{ij}=\sum_i\frac{\left[1+\left(\frac{\mu_i}{\mu_j}\right)^{\frac{1}{2}}\left(\frac{M_{w,j}}{M_{w,i}}\right)^{\frac{1}{4}}\right]^2}{\left[8\left(1+\frac{M_{w,i}}{M_{w,j}}\right)\right]^{\frac{1}{2}}} \tag{11}$$

Species equation:

$$\left(u\frac{\partial m_i}{\partial x}+v\frac{\partial m_i}{\partial y}+w\frac{\partial m_i}{\partial z}\right)=D_{eff}\left(\frac{\partial^2 m_i}{\partial x^2}+\frac{\partial^2 m_i}{\partial y^2}+\frac{\partial^2 m_i}{\partial z^2}\right)+\varepsilon S_c \tag{12}$$

In the species equation, m_i denotes the mass fraction of the ith species; the calculations have included CH_3OH, H_2O, H_2, CO_2 and CO. In Eq. (12), D_{eff} is the effective diffusion coefficient based on the Stefan–Maxwell equations [36]. Eq. (13) is employed to describe the influence of the porosity on the diffusion coefficient

$$D_{eff}=D_k\varepsilon^{\tau} \tag{13}$$

The diffusion coefficient D_k for the methanol steam micro-reformer was derived from the Stefan–Maxwell equations which were used to calculate the mean effective binary diffusivity [19]. In this work, the porosity ε is expressed as 0.38 and 1.00, in the catalyst layer and the flow channel, respectively. S_c represents the source terms due to the chemical reaction in the catalyst layer. Therefore, S_c is zero in the flow channel. Furthermore, S_c differs according to the reactant gases in the catalyst layer.

$$S_c=M_{w,i}(R_{SR}+R_{rWGS})(\lambda_i''-\lambda_i') \tag{14}$$

where λ_i' and λ_i'' are the stoichiometric coefficient for reactant i and product i, respectively, in the reaction.

According to the chemical kinetics of Purnama et al. [37], the steam reforming reaction is much faster than the decomposition and water–gas-shift reaction. Therefore, only the steam reforming reaction, Eq. (15), and the reverse water–gas shift reaction, Eq. (16), are considered in this study.

$$CH_3OH+H_2O\xrightarrow{k_1}CO_2+3H_2 \tag{15}$$

$$CO_2+H_2\underset{k_{-2}}{\overset{k_2}{\leftrightarrow}}CO+H_2O \tag{16}$$

In this study, the model for methanol steam reforming is that used by Hsueh and collaborators [31,32], and the Arrhenius equation is used to calculate the concentration of reactant gases generated by the chemical reaction.

$$R_{SR}=k_1C_{CH_3OH}^{0.6}C_{H_2O}^{0.4}\exp\left(-\frac{E_a}{RT}\right) \tag{17}$$

$$R_{rWGS}=k_2C_{CO_2}C_{H_2}\exp\left(-\frac{E_a}{RT}\right)-k_{-2}C_{CO}C_{H_2O}\exp\left(-\frac{E_a}{RT}\right) \tag{18}$$

where the steam reforming reaction is a non-reversible reaction and the reverse water–gas-shift reaction is reversible. The constants k_1 and k_2 are the forward rate constants for the steam reforming reaction and the reverse water–gas-shift reaction, respectively. The constant k_{-2} is the backward rate constant for the water–gas-shift reaction.

To calculate the local temperature, the energy equations must be solved.

Energy equation:

$$\rho c_p\left(u\frac{\partial T}{\partial x}+v\frac{\partial T}{\partial y}+w\frac{\partial T}{\partial z}\right)=k_{eff}\left(\frac{\partial^2 T}{\partial x^2}+\frac{\partial^2 T}{\partial y^2}+\frac{\partial^2 T}{\partial z^2}\right)+\varepsilon S_t \tag{19}$$

In the energy equation, the effective thermal conductivity is given by

$$k_{eff}=\varepsilon k_f+(1-\varepsilon)k_s \tag{20}$$

where k_f is the fluid phase thermal conductivity, k_s the solid medium thermal conductivity and ε the porosity of the medium.

The source term S_t in the energy equation due to the chemical reactions is determined by

$$S_t=-(\Delta H_{SR}R_{SR}+\Delta H_{rWGS}R_{rWGS}) \tag{21}$$

Table 1
Parameters used in this study.

Channel width W (m)	1.0×10^{-3}
Channel height H (m)	1.0×10^{-3}
Catalyst layer thickness δ_1 (m)	5.0×10^{-5}
Flow channel height δ_2 (m)	9.5×10^{-4}
Average inlet temperature (°C)	120
Operating pressure (atm)	1
Catalyst density (kg m^{-3}) [19]	1480
Catalyst thermal conductivity (W m^{-1} k^{-1}) [19]	0.3
Activation energy for steam reforming (J mol^{-1}) [20]	7.6×10^{4}
Activation energy for reverse water gas shift (J mol^{-1}) [20]	1.08×10^{5}
Catalyst layer porosity [23]	0.38
Catalyst permeability (m^2) [23]	2.379×10^{-12}
Mass diffusion coefficient (m^2 s^{-1}) [19]	6.8×10^{-5}

where ΔH_{SR} is the enthalpy of reaction of the steam reforming reaction, and ΔH_{rWGS} is the enthalpy of reaction of the reverse water–gas-shift reaction.

In the solid regions, the energy transport equation can be written as

$$\frac{\partial^2 T}{\partial x^2}+\frac{\partial^2 T}{\partial y^2}+\frac{\partial^2 T}{\partial z^2}=0 \tag{22}$$

The boundary conditions of the present computation include those at the inlet, outlet, wall, and the interfaces between the flow channel and the catalyst layer.

(1) The boundary conditions for inlets at the flow channel and the catalyst layer. The inlet flow velocity is constant, the inlet gas composition is constant, and the inlet temperature is constant.
(2) The boundary conditions for outlets at the flow channel and the catalyst layer. There is fully developed flow.
(3) The boundary conditions for the interface between the solid wall and the insulated walls. The temperature gradients are zero.
(4) The boundary conditions for the interface between the flow channel and the insulated walls. The velocities, temperature, temperature gradient, species concentration and species flux are zero.
(5) The boundary conditions for the interface between the flow channel and solid wall. No slip and zero fluxes hold the velocities and the concentration gradients at zero.
(6) The boundary conditions for the interface between the flow channel and the catalyst layer. The velocities, temperature, species concentration and species flux are continuous.
(7) The boundary conditions for the interface between the heated wall and the catalyst layers. The velocities and the concentration gradient are assumed to be zero, and the temperature is assumed to be equal to the constant wall temperature.

Fig. 1 presents schematics of the three-dimensional plate methanol steam micro-reformer considered in this work. The inlet cross-section of the channel is 1 mm × 1 mm. The thicknesses of the catalyst layers are set at 50 μm. The base conditions of the properties are as follows; the operating pressure is 1 atm and the inlet temperature is 120 °C. The inlet flow velocity is 1 m s^{-1} and the molar ratio of H_2O/CH_3OH is 1.3 in the first example. The physical properties of the channels are listed in Table 1.

3. Numerical method

The solution to the governing equations is obtained by employing a finite volume scheme with the model domain divided into a

Table 2
Temperature distributions (°C) for the various grid tests at different axial locations.

$I \times J \times K$	X						
	0	0.152	0.303	0.455	0.606	0.758	0.909
$67 \times 16 \times 3$	120	176	202	218	224	227	228
$133 \times 26 \times 5$	120	174	201	217	224	227	228
$265 \times 36 \times 9$	120	169	200	216	223	226	228

number of cells and used as control volumes. The governing equations are numerically integrated over each of these computational cells or control volumes. The method exploits a collocated cell-centered variable arrangement with the local or cell-averaged values of the physical quantities evaluated and stored at each cell center.

A generalized form of the transport equation for mass, momentum, energy can be expressed in a conservative form as follows:

$$\nabla \cdot (\rho \phi V) = \nabla \cdot (\Gamma \nabla \phi) + S_\phi \tag{23}$$

where ϕ is a general dependent variable, V is the velocity vector, S_ϕ is the source per unit volume and ρ is the density. With the discretization of the governing equations, the coupled finite-difference equations become

$$a_P \phi_P = a_E \phi_E + a_W \phi_W + a_N \phi_N + a_S \phi_S + S_\phi \tag{24}$$

where ϕ_P is the value of ϕ at the current point P, $\phi_E, \ldots, \phi_S$ stand for the values of the grid points adjacent to the point P, and $a_P, \ldots, a_S$ are known as the link coefficients. All equations were numerically solved using the commercial fluid dynamics program Fluent 6.1. The SIMPLE algorithm was employed to solve the convection–diffusion equations. The convergence criteria for the normalized residuals for each variable were restricted to be less than 10^{-6}.

In order to study the effect of grid number on the numerical results, the grid independence was examined in preliminary test runs. For simplification of the analysis, three grid configurations were evaluated for the single channel of the plate methanol steam micro-reformer at a wall temperature of 230 °C. The single channel length is 33 mm, and the cross-section of the channel is 1 mm × 1 mm. The thicknesses of the catalyst layer are set at 50 μm. The inlet flow velocity is 1 m s^{-1} and the molar ratio of H_2O/CH_3OH is 1.3. The physical properties of the channel are listed in Table 1. The numbers of grid lines in the x, y and z directions were $265 \times 36 \times 9$, $133 \times 26 \times 5$, and $67 \times 16 \times 3$. The influence of grid lines on the local temperatures is shown in Table 2. The deviations of local temperatures are 0.04–1.1% for grids $67 \times 16 \times 3$ and $133 \times 26 \times 5$, and 0.4–2.8% for grids $133 \times 26 \times 5$ and $265 \times 36 \times 9$. Therefore, Grid $132 \times 25 \times 4$ was chosen for the simulation in the present study as a tradeoff between accuracy and CPU computation time.

In order to compare the numerical results and experimental data, a micro-reformer with parallel flow field is tested. Fig. 2 shows a comparison of the present prediction with previous experimental data. The solid symbols denote the experimental results of Park et al. [38] and the curve is the present prediction. Only small discrepancies between the numerical results and the experimental data have been found. The numerical model accurately predicted the methanol conversion and the gas distributions. Hence, the proposed three-dimensional numerical model is adequate for analyzing the heat and mass transfer in a micro-reformer.

4. Results and discussion

In past studies of heat and mass transfer in a micro-reformer, simplified models without wall conduction effects have been developed. In this work, a detailed analysis of the three-dimensional modeling with wall conduction effects has been proposed

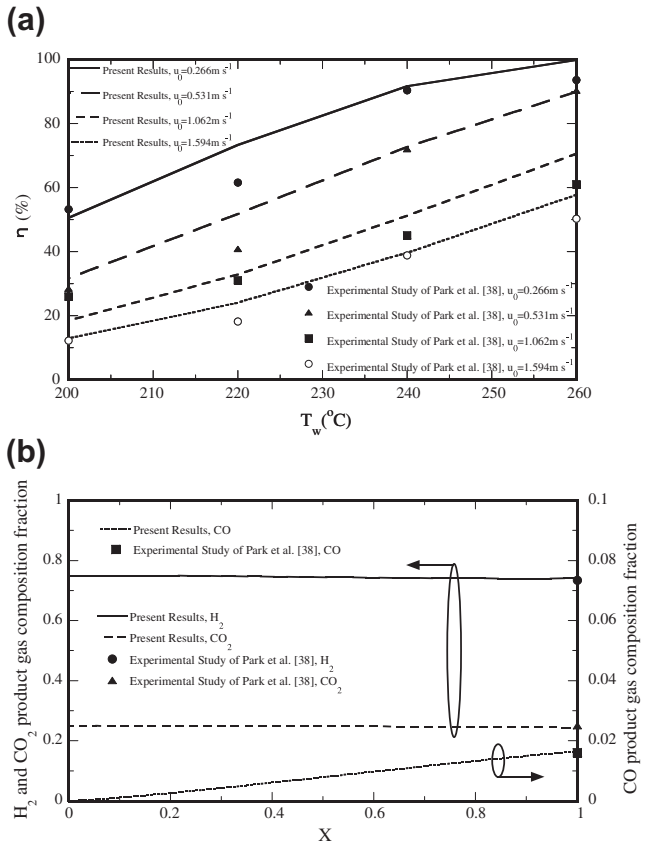

Fig. 2. Comparison of present prediction with the previous experimental data of Park et al. [38]. (a) Methanol conversion and (b) product gas composition.

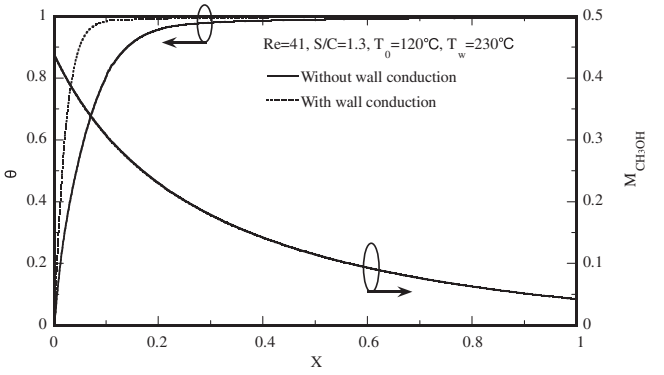

Fig. 3. Comparisons of the predicted results with and without wall conduction effects for the temperature distributions and CH_3OH mole fraction distributions along the centerline of the serpentine flow field ($Y = 0.5$).

to examine the transport phenomena of heat and mass transfer in a micro-reformer with serpentine flow channels. Fig. 3 presents the effects of wall conduction on the local temperature distributions and CH_3OH mole fraction distributions along the centerline of the serpentine flow field. In this plot, X denotes the dimensionless distance from the serpentine flow channel inlet to outlet. It is clearly seen that the temperature distribution is affected by the wall thermal conduction and shows a rapid and uniform development compared with that without a wall conduction effect. This implies that the effects of wall conduction on the thermal development in a micro-reformer are important. In addition, it is found in Fig. 3 that the effects of wall conduction on the methanol

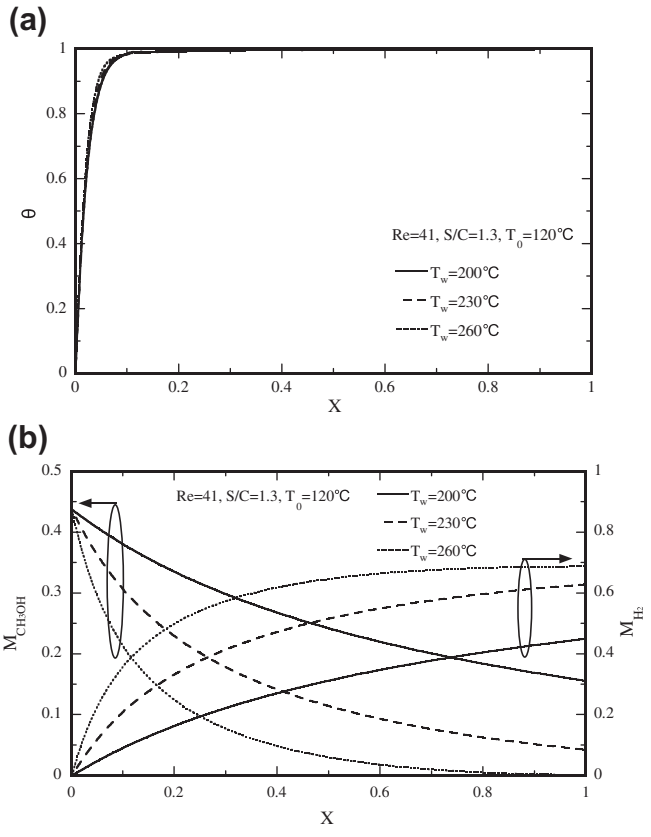

Fig. 4. Effects of various wall temperatures on: (a) the temperature distributions and (b) the CH_3OH mole fraction distributions along the centerline of the serpentine flow field ($Y = 0.5$).

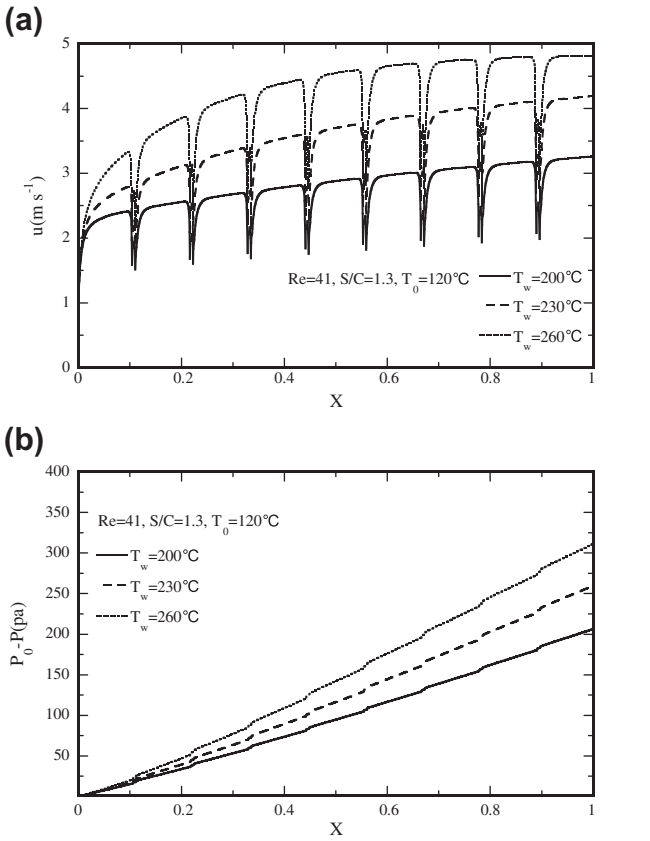

Fig. 5. Effects of various wall temperatures on: (a) the local velocity and (b) the local pressure along the centerline of the serpentine flow field ($Y = 0.5$).

distribution are negligible, whereas their effect on the temperatures distribution is remarkable and cannot be neglected in the modeling. Therefore, wall conduction effects are taken into account in this work.

The wall temperature, T_w, on the heated wall is important. To this end, the effects of wall temperatures on the dimensionless temperature distributions along the centerline of the serpentine flow field at a Reynolds number of 41 and a H_2O/CH_3OH molar ratio of 1.3 are examined in Fig. 4a. In Fig. 4a, the fluid temperature shows a significant increase when the fuel moves downstream. The fluid temperature increases along the serpentine flow channel due to the heated wall. The dimensionless temperature experiences a negligible variation when $X > 0.3$. This is due to thermal equilibrium for $X > 0.3$, in which the temperature has a more uniform distribution. In addition, it is found in Fig. 4a that the dimensionless temperature distributions are almost the same for various values of wall temperature. Fig. 4b shows the effects of the wall temperature T_w on the distribution of CH_3OH and H_2 mole fraction along the centerline of the serpentine flow field. The CH_3OH mole fraction gradually decreases along the flow directions due to the chemical reaction, whereas the H_2 mole fractions increase when the flow moves downstream. It is also clearly seen that the CH_3OH consumption and the H_2 mole fractions increase with an increase in the wall temperature. A lower CH_3OH mole fraction and a higher H_2 mole fraction along the serpentine flow field represent a higher methanol conversion.

The velocity distributions along the centerline of the serpentine flow field for various values of wall temperature are presented in Fig. 5a. Significant variations are seen clearly at the turning points of the flow channel due to the change of velocity direction. The fuel flow velocity increases from the inlet to outlet, due to increases in the temperature caused by significant density variation. The rise in fuel velocity becomes relatively insignificant since it is fully developed thermally at $X > 0.3$. The thermo-fluid parameters affect not only the methanol conversion efficiency, but also pressure loss (the difference between local and inlet pressures) in the serpentine flow channel. Large pressure drops in the channel mean that more pumping work is needed to pump the reactants. Thus, pressure loss is a significant issue. An exploration of pressure loss for various wall temperatures along the centerline of the serpentine flow field is presented in Fig. 5b. Local pressure loss increases along the serpentine flow field. A larger pressure loss occurs at higher wall temperatures. In addition, clearly observed variations in the pressure loss appear at the turning points, due to the velocity change. The pressure losses are higher for the serpentine flow field than for the parallel flow channel [32], so reducing them is a priority for future use with the plate methanol micro-reformer.

The effects of the Reynolds number (Re) on the local dimensionless temperature, CH_3OH and H_2 mole fraction distributions at $T_w = 230\,^{\circ}C$ are analyzed in Fig. 6. A careful examination of Fig. 6a reveals that the dimensionless temperature increases as the fluid moves downstream due to the heated wall. In addition, the dimensionless temperature rise is lower for a higher Re. This is due to the fact that a higher Reynolds number significantly increases the heat leaving the flow channel, which decreases the temperature rise. In Fig. 6b, the CH_3OH mole fraction clearly decreases along the serpentine flow field. This is due to the temperature rise caused by the strong chemical reaction, which in turn increases the methanol consumption. Also, the methanol mole fraction distributions decrease with a lower Reynolds number. The results also show that a higher H_2 mole fraction is noted for the lower Reynolds number. This is due to the longer gas resident

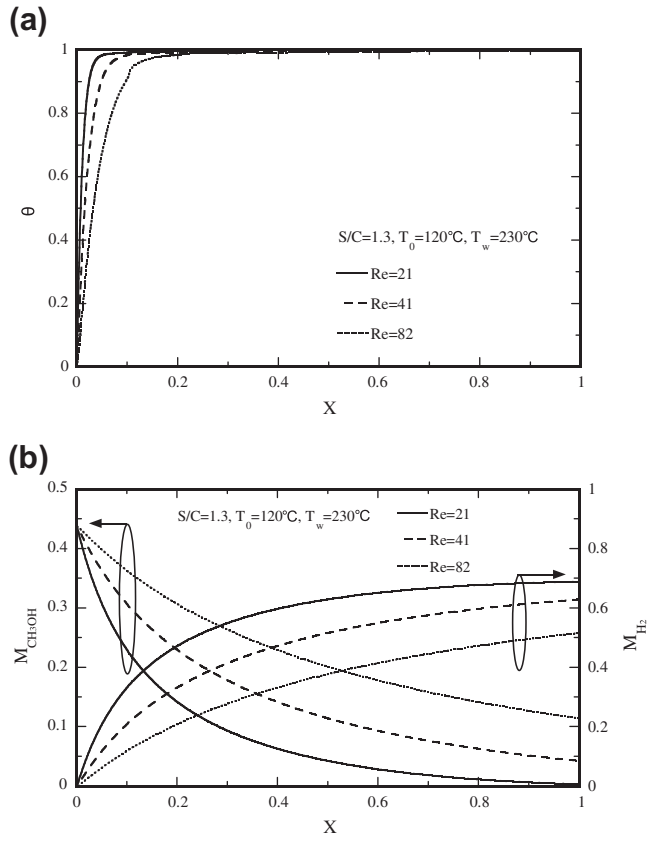

Fig. 6. Effects of Reynolds numbers at $T_w = 230\ ^\circ C$ on: (a) the temperature distributions and (b) the CH_3OH mole fraction distributions along the center line of the serpentine flow field ($Y = 0.5$).

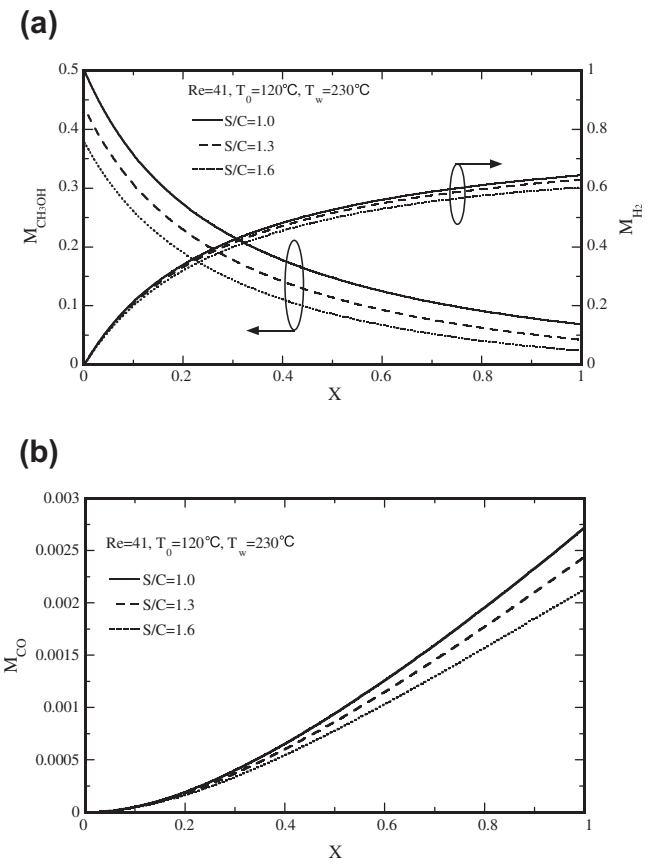

Fig. 7. Effects of H_2O/CH_3OH molar ratio (S/C) at $T_w = 230\ ^\circ C$ on: (a) the temperature distributions and (b) the CH_3OH mole fraction and CO mole fraction distributions along the center line of the serpentine flow field ($Y = 0.5$).

time which results in a better methanol conversion and a higher H_2 production.

Fig. 7 presents the effects of the H_2O/CH_3OH (S/C) molar ratio on the CH_3OH, H_2 and CO mole fraction distributions at $T_w = 230\ ^\circ C$. Fig. 7a shows that more efficient methanol conversion is noted at a higher H_2O/CH_3OH molar ratio. It is also found that a higher molar ratio of H_2O/CH_3OH causes the H_2 mole fraction to fall. The CO mole fraction distributions are also shown in Fig. 7b. The CO concentration decreases with an increase in H_2O/CH_3OH molar ratio. This is because the higher H_2O concentration would enhance the water–gas-shift reaction, which in turn reduces the CO concentration. However, the higher H_2O/CH_3OH molar ratio also reduces the H_2 concentration at the channel outlet.

Figs. 8 and 9 present the CH_3OH, H_2 and CO mole fraction distributions for $T_w = 230\ ^\circ C$ along the middle cross-section of the serpentine flow field ($Y = 0.5$) and the interface between flow channel and catalyst layer ($Y = 0.95$), respectively. An overall inspection of Figs. 8 and 9 reveals that the mole fraction of CH_3OH decreases along both the middle cross-section of the channel and the interface between the flow channel and catalyst layer. A comparison between Figs. 8 and 9 show that the methanol consumption is higher at the interface compared with the middle cross-section. This is because the interface has a higher temperature and chemical reaction rate. It is evident that the mass fraction of H_2 and CO increases along the middle cross-section of the serpentine flow field and along the interface between the flow channel and catalyst layer. This confirms that a methanol micro-reformer with a higher CH_3OH consumption indicates a higher H_2 and CO concentration, as would be expected.

Fig. 10 presents the effects of the Reynolds number Re on the methanol conversion η and H_2 production rate Q_{H2} for various values of wall temperature T_w. In Fig. 10, the value of Q_{H2} increases and η decreases with an increase in Re. This can be attributed to the fact that a lower Re implies an increase in the fuel residence time and temperature distributions in the micro-reformer, which in turn improves the methanol conversion. As for the Q_{H2}, a higher Q_{H2} is found for the case with a higher Re due to the higher inlet flow rate. In addition, η and Q_{H2} increase with an increase in wall temperature T_w. Besides, it is important to note that a higher Reynolds number will not necessarily provide a better H_2 production rate. When the methanol conversion is too small, a higher Reynolds number may provide a lower H_2 production rate.

The effects of various heated plates of the channel on the temperature distributions and CH_3OH mole fraction distributions are examined in Fig. 11. In Fig. 11, two cases of heated plates were tested, top heated plate ($Y = 1$) or bottom heated plate ($Y = 0$). The effects of top versus bottom heated plates of the channel on temperature distributions along the center line of the serpentine flow field are shown in Fig. 11. A top heated plate has a higher temperature distribution than a bottom heated plate. This is because a bottom heated plate has a smaller temperature rise due to fuel convection effects, while a top heated plate with the heated position near the catalyst layer has a more significant temperature rise. For a bottom heated plate, it is also apparent that marked temperature variations occur at the turning points of the flow channel due to the change of the heat flow direction. The top heated plate clearly has a larger methanol consumption than the bottom heated plate. These phenomena make it obvious that the stronger chemical reaction for the case with the top heated plate is due to a higher temperature distribution.

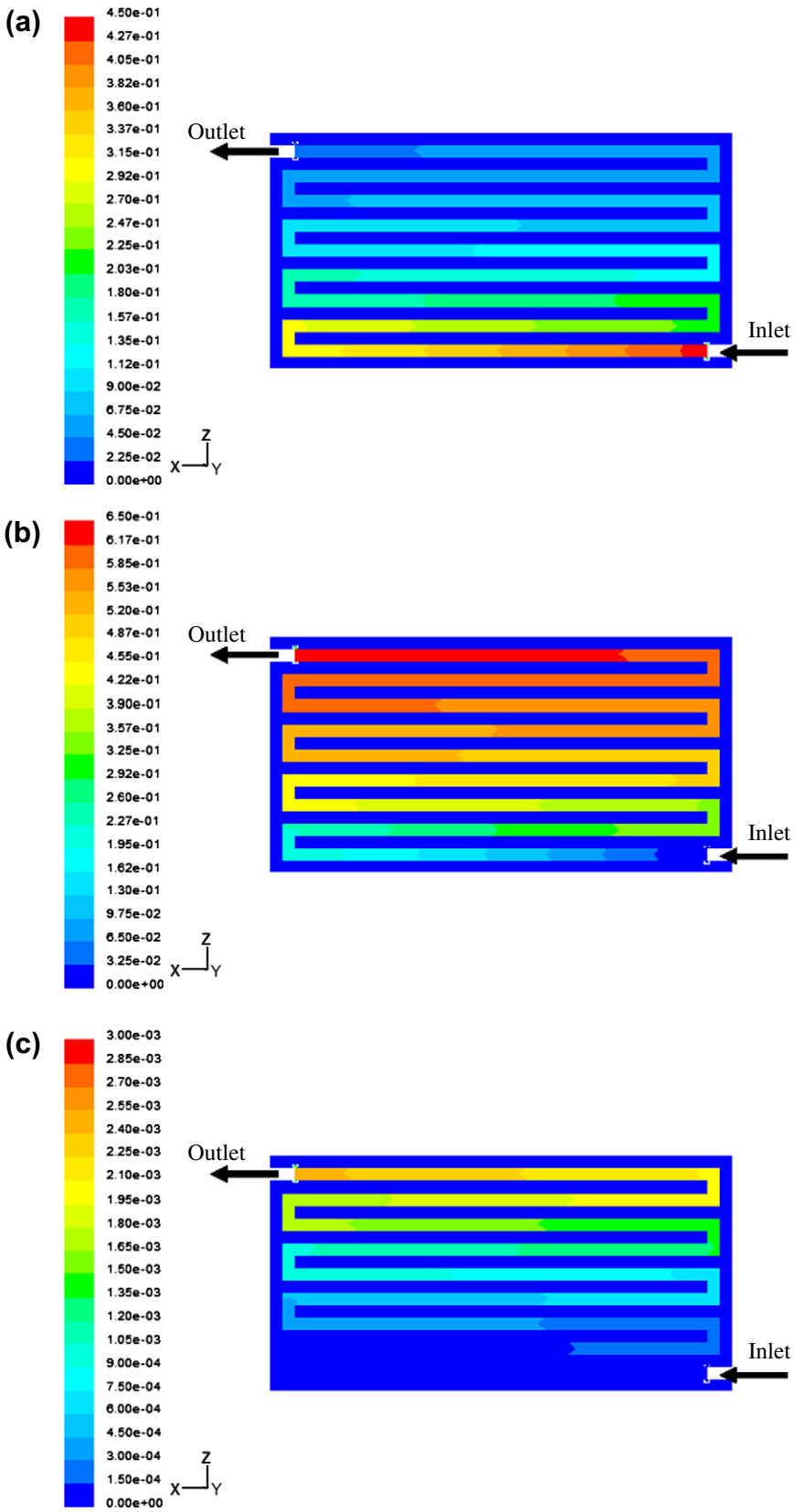

Fig. 8. Local distributions of: (a) CH_3OH mole fraction, (b) H_2 mole fraction and (c) CO mole fraction along the cross-section of $Y = 0.5$ at $T_w = 230$ °C.

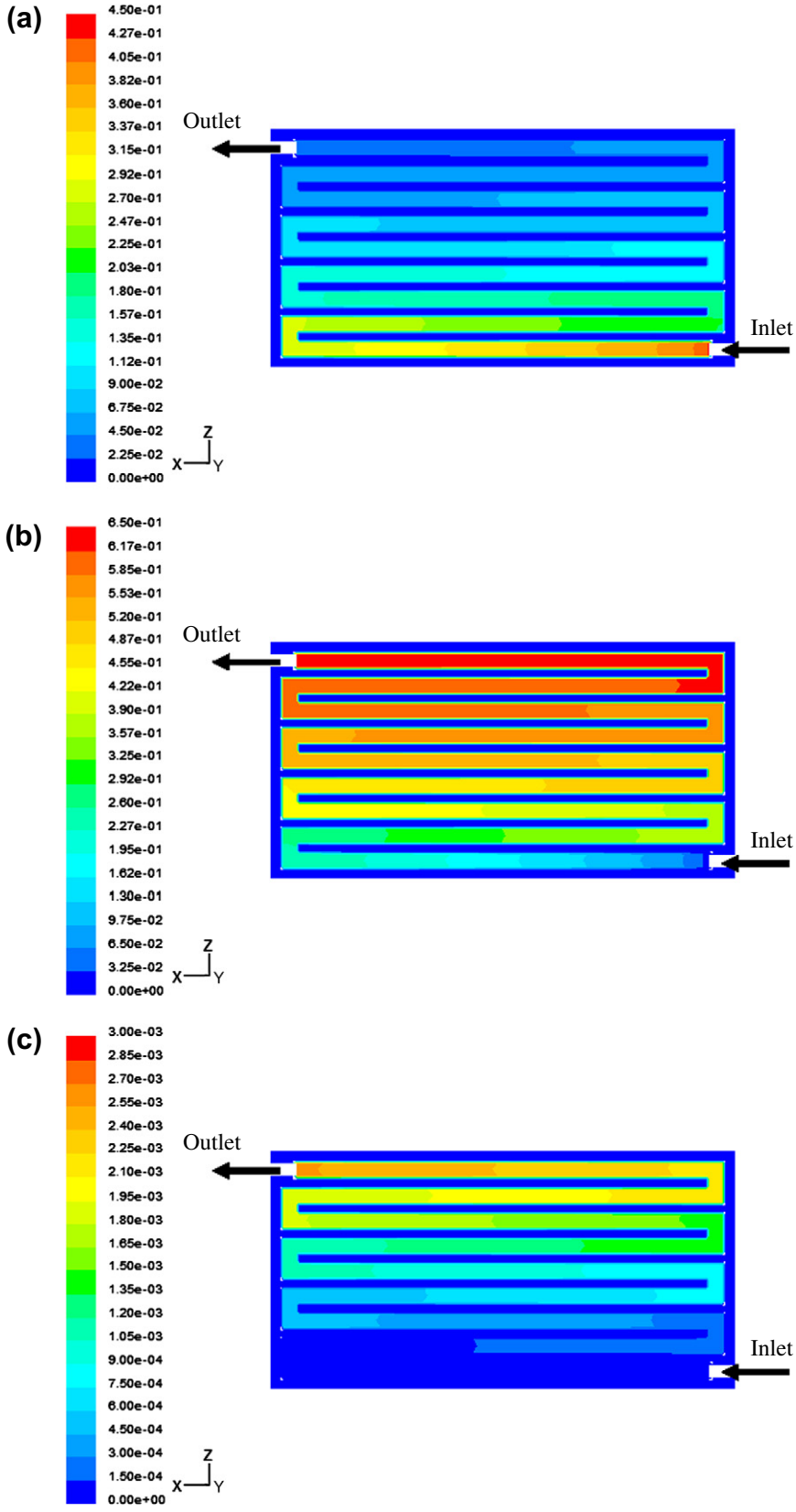

Fig. 9. Local distributions of: (a) CH_3OH mole fraction, (b) H_2 mole fraction and (c) CO mole fraction along the interface between the flow channel and catalyst layer ($Y = 0.95$) at $T_w = 230°$.

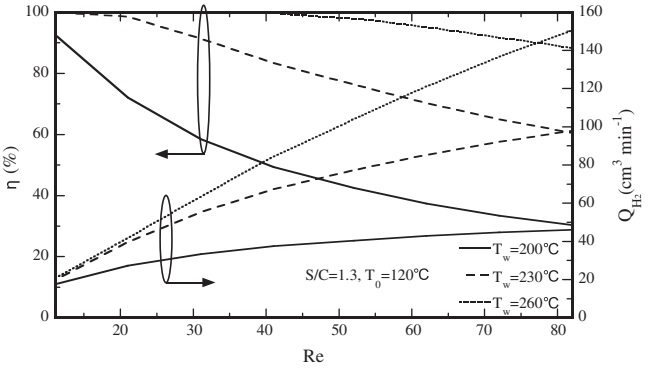

Fig. 10. Effects of wall temperature and inlet fuel Reynolds number on the methanol conversion and H_2 production rate.

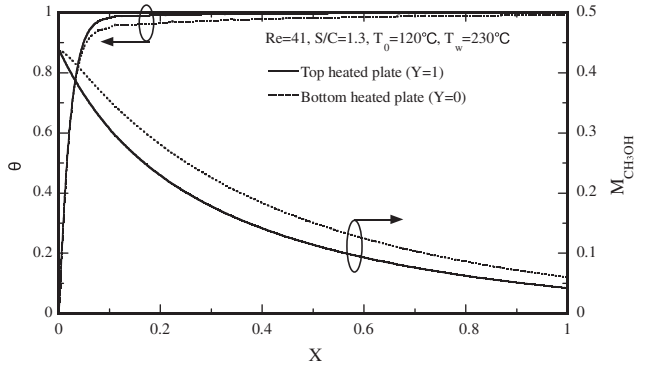

Fig. 11. Effects of heating different channel plates on the temperature and CH_3OH mole fraction distributions along the center line of the serpentine flow field ($Y = 0.5$).

5. Conclusions

A three-dimensional heat and mass transfer of micro-reformer with the serpentine flow field numerical model is developed to examine the effects of various values of wall temperature, fuel ratio and Reynolds number on the plate methanol steam micro-reformer performance and local transport phenomena. The conclusions drawn from the analysis are:

1. The predictions with and without wall conduction effects show that this has a significant impact on the thermal development and a negligible effect on the chemical reactions.
2. The prediction shows that the methanol conversion increases with an increase in wall temperature T_w. The methanol conversion for $T_w = 260$ °C could be improved by 53% relative to that of $T_w = 200$ °C.
3. A reduced Reynolds number for the reactant gas in the channel would raise the reactant gas residence time and yield more uniform temperature distributions, which in turn increases the reaction time and improves the methanol conversion efficiency.
4. The CO concentration would be reduced from 0.27% to 0.21% at $T_w = 230$ °C as the H_2O/CH_3OH molar ratio value is increased from 1.0 to 1.6.
5. By comparing the predicted results with top or bottom heated condition, it indicates that the methanol conversion for the condition with the top heated plate could be improved by 4.4%.

Acknowledgement

The study was supported by the National Science Council, the Republic of China, through the Grants NSC 97-2221-E-211-015-MY2.

References

[1] Baschuk JJ, Li X. A comprehensive, consistent and systematic mathematical model of PEM fuel cells. Appl Energy 2009;86:181–93.
[2] Henriques T, César B, Costa Branco PJ. Increasing the efficiency of a portable PEM fuel cell by altering the cathode channel geometry: a numerical and experimental study. Appl Energy 2010;87:1400–9.
[3] Perng SW, Wu HW. Effect of the prominent catalyst layer surface on reactant gas transport and cell performance at the cathodic side of a PEMFC. Appl Energy 2010;87:1386–99.
[4] Perng SW, Wu HW, Jue TC, Cheng KC. Numerical predictions of a PEM fuel cell performance enhancement by a rectangular cylinder installed transversely in the flow channel. Appl Energy 2009;86:1541–54.
[5] Kundu A, Jang JH, Gil JH, Jung CR, Lee HR, Kim SH, et al. Micro-fuel cells-current development and applications. J Power Sources 2007;170:67–78.
[6] Pfeifer P, Schubert K, Liauw MA, Emig G. Electrically heated microreactors for methanol steam reforming. IChemE 2003;81:711–20.
[7] Lim MS, Kim MR, Noh J, Woo SI. A plate-type reactor coated with zirconia-sol and catalyst mixture for methanol steam-reforming. J Power Sources 2005;140:66–71.
[8] Kwon OJ, Hwang SM, Chae JH, Kang MS, Kim JJ. Performance of a miniaturized silicon reformer-PrOx-fuel cell system. J Power Sources 2007;165:342–6.
[9] Sohn JM, Byun YC, Cho JY, Choe J, Song KH. Development of the integrated methanol fuel processor using micro-channel patterned devices and its performance for steam reforming of methanol. Int J Hydrogen Energy 2007;32:5103–8.
[10] Ha JW, Jang JH, Gil JH, Kim SH. The fabrication and performance of a poly(dimethylsiloxane) (PDMS)-based microreformer for application to electronics. Int J Hydrogen Energy 2008;33:2059–63.
[11] Park GG, Yim SD, Yoon YG, Kim CS, Seo DJ, Eguchi K. Hydrogen production with integrated microchannel fuel processor using methanol for portable fuel cell systems. Catal Today 2005;110:108–13.
[12] Won JY, Jun HK, Jeon MK, Woo SI. Performance of microchannel reactor combined with combustor for methanol steam reforming. Catal Today 2006;111:158–63.
[13] Park DE, Kim T, Kwon S, Kim CK, Yoon E. Micromachined methanol steam reforming system as a hydrogen supplier for portable proton exchange membrane fuel cells. Sens Actuat A 2007;135:58–66.
[14] Kwon OJ, Yoon DH, Kim JJ. Silicon-based miniaturized reformer with methanol catalytic burner. Chem Eng J 2008;140:466–72.
[15] Kim T, Kwon S. MEMS fuel cell system integrated with a methanol reformer for a portable power source. Sens Actuat A 2009;154:204–11.
[16] Suh JS, Lee MT, Greif R, Grigoropoulos CP. A study of steam methanol reforming in a microreactor. J Power Sources 2007;173:458–66.
[17] Suh JS, Lee MT, Greif R, Grigoropoulos CP. Transport phenomena in a steam–methanol reforming microreactor with internal heating. Int J Hydrogen Energy 2009;34:314–22.
[18] Karim A, Bravo J, Datye A. Nonisothermality in packed bed reactors for steam reforming of methanol. Appl Catal A 2005;282:101–9.
[19] Karim A, Bravo J, Gorm D, Conant T, Datye A. Comparison of wall-coated and packed-bed reactors for steam reforming of methanol. Catal Today 2005;110:86–91.
[20] Pan L, Wang S. Modeling of a compact plate-fin reformer for methanol steam reforming in fuel cell systems. Chem Eng J 2005;108:51–8.
[21] Liu N, Yuan Z, Wang C, Pan L, Wang S, Li S, et al. A plate-type reactor coated with zirconia-sol and catalyst mixture for methanol steam-reforming. Chem Eng J 2008;139:56–62.
[22] Pattekar AV, Kothare MV. A radial microfluidic fuel processor. J Power Sources 2005;147:116–27.
[23] Pattekar AV, Kothare MV. A microreactor for hydrogen production in micro fuel cell applications. J Microelectromech Syst 2004;13:7–18.
[24] Cao C, Wang Y, Holladay JD, Jones EO, Palo DR. Design of micro-scale fuel processors assisted by numerical modeling. AIChE J 2005;51:982–8.
[25] Stamps AT, Gatzke EP. Dynamic modeling of a methanol reformer-PEMFC stack system for analysis and design. J Power Sources 2006;161:356–70.
[26] Yoon HC, Otero J, Erickson PA. Reactor design limitations for the steam reforming of methanol. Appl Catal B 2007;75:269–76.
[27] Arzamendi G, Dieguez PM, Montes M, Odriozola JA, Sousa-Aguiar EF, Gandia LM. Methane steam reforming in a microchannel reactor for GTL intensification: A computational fluid dynamics simulation study. Chem Eng Sci 2009;154:168–73.
[28] Arzamendi G, Dieguez PM, Montes M, Centeno MA, Odriozola JA, Gandia LM. Integration of methanol steam reforming and combustion in a microchannel reactor for H_2 production: a CFD simulation study. Catal Today 2009;143:25–31.
[29] Varesano A, Guaglio I, Saracco G, Maffettone PL. Dynamics of a methanol reformer for automotive applications. Ind Eng Chem Res 2005;44:759–68.

[30] Kundu A, Jang JH, Lee HR, Kim SH, Gil JH, Jung CR, et al. MEMS-based micro-fuel processor for application in a cell phone. J Power Sources 2006;162:572–8.
[31] Chen F, Chang MH, Kuo CY, Hsueh CY, Yan WM. Analysis of a plate-type microreformer for methanol steam reforming reaction. Energy Fuels 2009;23:5092–8.
[32] Hsueh CY, Chu HS, Yan WM. Numerical study on micro-reformer performance and local transport phenomena of the plate methanol steam micro-reformer. J Power Sources 2009;187:535–43.
[33] Kim T, Kwon S. Design, fabrication and testing of a catalytic microreactor for hydrogen production. J Micromech Microeng 2006;16:1760–8.
[34] Park HG, Malen JA, Piggott III WT, Morse JD, Greif R, Grigoropoulos CP. Methanol steam reformer on a silicon wafer. J Microelectromech Syst 2006;15:976–85.
[35] Ergun S. Fluid flow through packed columns. Chem Eng Prog 1952;48:89–94.
[36] White FM. Viscous fluid flow. 2nd ed. McGraw-Hill; 1991.
[37] Purnama H, Ressler T, Jentoft RE, Soerijanto H, Schlogl R, Schomacker R. CO formation/selectivity for steam reforming of methanol with a commercial $CuO/ZnO/Al_2O_3$ catalyst. Appl Catal A 2004;259:89–94.
[38] Park GG, Seo DJ, Park SH, Yoon YG, Kim CS, Yoon WL. Development of microchannel methanol steam reformer. Chem Eng J 2004;101:87–92.